

Signatures of Molecular Orientation and Orbital Symmetry in Strong-Field Photoelectron Angular and Energy Distributions of Diatomic Molecules and Small Carbon Clusters

A. Jaroń-Becker^{1,2}, A. Becker¹, and F. H. M. Faisal³

¹ Max-Planck-Institut für Physik komplexer Systeme, Nöthnitzer Str. 38, Dresden, D-01187 Germany

e-mail: abecker@mpipks-dresden.mpg.de

² Institute for Theoretical Physics, Warsaw University, Hoza 69, Warsaw, 00-691 Poland

³ Fakultät für Physik, Universität Bielefeld, Postfach 100131, Bielefeld, D-33501 Germany

Received September 15, 2003

Abstract—Using a leading order intense-field S-matrix analysis, we study the angular and energy distribution of the photoelectron for multiphoton ionization of diatomic molecules and linear carbon clusters. We show that alignment of molecules can be simply determined from the observation (i) of a nodal minimum along the laser polarization direction in the photoelectron angular distributions for molecules with active π electrons or (ii) of a minimum in the above threshold ionization spectra of homonuclear diatomics at high energies. The origins, as well as the conditions under which these signatures can be observed in the experiment, are discussed.

1. INTRODUCTION

The past decade has witnessed a growing interest in using laser fields to control the outcome of chemical reactions [1]. In order to enable control of complex reactions, a deep understanding of basic processes, such as single electron ionization, is necessary. Compared with the atomic case, the physics of laser–molecule interactions is enriched and complicated by the presence of other nuclei, which break the spherical symmetry of the binding potential and introduce dissociation as an additional channel of disintegration. Consequently, in the study of the multiphoton ionization of molecules, two aspects, new in comparison to the atomic case, have to be taken into account, namely, the symmetry of the wavefunction of the molecule and the orientation of the molecular axis/plane in space.

Concerning molecular symmetry, recently it has been established that the symmetry of the highest occupied molecular orbital (HOMO) influences the low-energy part of the energy spectrum [2] and the total ion yield [3, 4] of homo-nuclear diatomic and symmetric polyatomic molecules. This is due to the destructive or constructive interference of the electronic wave packets originating from the atomic centers within the molecule. For example, it has been shown that the antibonding symmetry of the HOMO in O_2 gives rise to destructive interference between the two subwaves, which leads to a suppression of the low-energy part of the above threshold ionization (ATI) spectrum [2] and, consequently, of the total ion yields [3]. Further signatures of molecular symmetry have been identified in the yields of doubly ionized polyatomic molecules and its fragments [5], in high harmonic spectra of diatomics [6] and ring-shaped molecules [7], and in high-order

ATI spectra of diatomics [8]. Very recently, photoelectron angular distributions were also studied in this context [9, 10].

A laser field can be used to control the external degrees of freedom of molecules on a microscopic level. In this respect, the spatial alignment of molecules is of much interest due to a variety of possible applications [11, 12], such as control of ionization and dissociation pathways, rotational cooling, molecular trapping and focusing, pendular-state spectroscopy, the study of steric effects in chemical reaction dynamics, and possible control of the outcome of chemical reactions. There are several methods of controlling the molecular alignment. For example, polar molecules can be oriented by electrical hexapole focusing [13] or through orientation of a strong dc electrical field [14]. Alignment of polar and nonpolar molecules can be also achieved using intense laser pulses [11, 12, 15, 16].

To establish molecular alignment in short laser pulses, it is crucial to identify signatures of alignment experimentally. Such a signature has been found, for example, in multielectron dissociative ionization processes [11, 16–18], where ionic fragments are emitted preferentially along the direction of polarization of a (linearly polarized) laser field. Identification of alignment in such experiments requires discrimination [12, 18, 19] between the anisotropies observed on the one hand due to laser-induced reorientation of the molecule prior to ionization/dissociation (so-called dynamic alignment) and that on the other hand due to the angular dependence of the ionization process (so-called geometric alignment). Another method is to look for the change in the photoelectron angular distribution due to molecular alignment in an intermediate excited bound

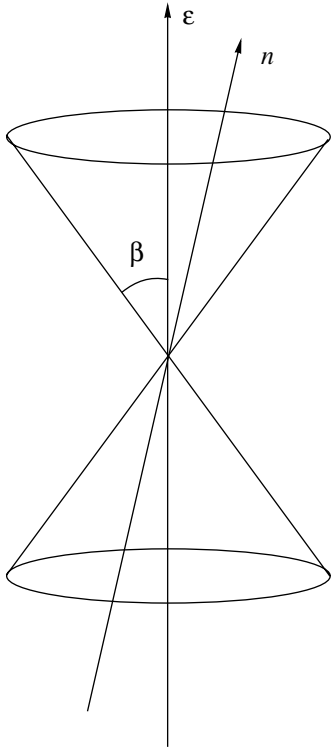


Fig. 1. Definition of the cone angle β used in the analysis of the sensitivity of the signatures of molecular orientation on the degree of alignment.

state occurring in a REMPI (resonant multiphoton ionization) process [20].

In this paper, we describe alternative signatures of alignment and molecular orbital symmetries in the photoelectron angular and energy distributions of classes of neutral linear molecules exposed to an ultrashort intense laser field. Since, to observe these signatures, neither fragmentation nor a specific intermediate resonance wavelength is involved, this method is complementary to those used previously. The paper is organized as follows: in the next section, the theory used in our calculations is described, and in the two further sections results are presented for the photoelectron angular distributions and energy distributions.

2. THEORY

All results were obtained using an extension of the Keldysh–Faisal–Reiss (KFR) theory [21] to the ionization of molecules [2–4]. It corresponds to the leading order of the *ab initio* intense-field S-matrix theory and involves nonresonant transitions of a molecule from the initial electronic ground state to the final state of the molecular ion and the field-dressed Volkov electron (e.g., [22]).

The angular distribution of the ejected electrons can be given in terms of the differential rate of ionization

per element of solid angle $d\Omega$ along the axis of electron detection as follows [3, 4, 9]:

$$\frac{dW(I, \hat{n})}{d\Omega} = N_e 2\pi \left(\frac{(2I_p)^2}{E_0} \right)^{\frac{3}{2}} \sqrt{\frac{2Z}{\sqrt{2I_p}}} \quad (1)$$

$$\times \sum_{N=N_0}^{\infty} k_N (U_p - N\omega)^2 J_N^2 \left(\alpha_0 \cdot \mathbf{k}_N; \frac{U_p}{2\omega} \right) \left| \langle \phi_{\mathbf{k}_N} \phi_f^+ | \phi_i \rangle (\hat{n}) \right|^2,$$

where \hat{n} is an unit vector along the molecular axis, N_e is the number of electrons in the active molecular orbital, $Z = 1$ is the charge state of the molecular ion, E_0 is the peak field strength of the laser and I_p is the ionization energy of the molecule. $J_N(a; b)$ is a generalized Bessel function of two arguments (e.g., [22]), where $\alpha_0 = \sqrt{I}/\omega$ is the quiver radius and $U_p = I/4\omega^2$ is the quiver energy of an electron in a laser field of frequency ω and intensity I . $\phi_{\mathbf{k}_N}$ is a plane wave, and ϕ_i and ϕ_f^+ are the initial and final ground-state wavefunctions of the neutral molecule and the molecular ion, which are obtained from the quantum chemical software package GAMESS-US, within the Hartree–Fock approximation [23]. $k_N^2/2 = N\omega - U_p - I_p$ is the kinetic energy of an electron upon absorption of N photons from the field and N_0 is the minimum (or threshold) photon number that has to be absorbed for ionization.

In order to study the dependence of the distribution on the different degrees of alignment, we also consider the averaged angular distributions:

$$\frac{dW(I, \beta)}{d\Omega} = \frac{1}{2\pi\beta} \int_0^{2\pi} d\phi_{\hat{n}} \int_0^{\beta} d\theta_{\hat{n}} \sin\theta_{\hat{n}} \frac{dW(I, \hat{n})}{d\Omega}, \quad (2)$$

where β is depicted in Fig. 1 and denotes the maximum cone angle of alignment. In other words, we assume the molecular axes in an ensemble of molecules are evenly distributed within the cone.

The angular distribution of photoelectron yields is obtained by combining the fundamental rates, Eq. (1), with the rate equation

$$\frac{dP_{\Omega}(\mathbf{r}; t)}{dt} = \frac{dW(I(\mathbf{r}; t), \beta)}{d\Omega} (1 - \int d\Omega P_{\Omega}(\mathbf{r}; t)), \quad (3)$$

where $I(\mathbf{r}, t)$ is the space–time profile of the laser beam, and summing the contributions from all points in the laser focus. For the present calculations, we have used a Gaussian pulse profile centered around $t = 0$ and a TEM₀₀-mode Gaussian beam. We have restricted the spatial variation to the axis perpendicular to the direction of propagation. The latter corresponds to experimental situations in which the Rayleigh length of the laser beam is significantly larger than the dimensions of the time-of-flight spectrometer.

Similarly, one obtains the photoelectron energy distribution by calculating first the above-threshold-ionization rate on absorbing N photons:

$$W^{(N)}(I, \hat{n}) = N_e 2\pi \left(\frac{(2I_p)^3}{E_0} \right)^{\frac{2Z}{\sqrt{2}I_p 2\pi}} \int_0^\pi d\phi_{k_n} \quad (4)$$

$$\times \int_0^\pi d\theta_{k_n} \sin(\theta_{k_n}) J_N^2 \left(\boldsymbol{\alpha}_0 \cdot \mathbf{k}_N; \frac{U_p}{2\omega} \right) \left| \langle \phi_{\mathbf{k}_N} \phi_f^+ | \phi_i \rangle(\hat{n}) \right|^2.$$

As in case of angular distributions, we also investigate the influence of different orientations of the axes of molecules by averaging over the cone angle β :

$$W^{(N)}(I, \beta) = \frac{1}{2\pi\beta} \int_0^{2\pi} d\phi_{\hat{n}} \int_0^\beta d\theta_{\hat{n}} \sin\theta_{\hat{n}} W^{(N)}(I, \hat{n}). \quad (5)$$

The photoelectron energy spectra are then obtained by solving the following rate equations:

$$\frac{dP^{(N)}(\mathbf{r}, t, \hat{n})}{dt} = W^{(N)}(I(\mathbf{r}, t), \hat{n}) \left(1 - \sum_{N=N_0}^{\infty} P^{(N)}(\mathbf{r}, t, \hat{n}) \right). \quad (6)$$

The results for the ion yields and the above-threshold-ionization spectra obtained previously within this theory have been found to be in good agreement with the experimental data for N_2 , O_2 , C_2H_2 , C_2H_4 , and C_6H_6 [2–4]. In particular, the successful application to hydrocarbons lets us anticipate that the theory provides reliable predictions for carbon clusters as well.

The ionization potentials and internuclear distances for the diatomic molecules C_2 , N_2 , and O_2 were taken from [24]. The structures and equilibrium geometries of the carbon clusters have been a subject of heated discussion in the literature since the development of ab initio chemical programs. Only recently, mostly due to the increase in computer power, was an agreement on the equilibrium geometry obtained [25, 26]. We have made use of recent results for the vertical ionization potentials [27] and the structure of the carbon chains [25, 27]. Figure 2 shows the geometry and bond lengths of carbon clusters used in the present calculations.

3. RESULTS FOR PHOTOELECTRON ANGULAR DISTRIBUTIONS

We consider the angular distributions of photoelectrons emitted from an ensemble of molecules whose molecular axes are within a given cone angle. Angular distributions of photoelectrons resulting from the strong-field ionization of molecules were investigated for the first time in [9]. We are interested here in how sensitive the angular distributions and the symmetry

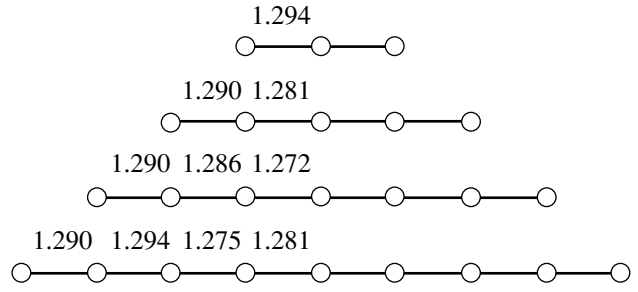


Fig. 2. Geometries and bond lengths (in Å) of linear carbon clusters used in the present calculations.

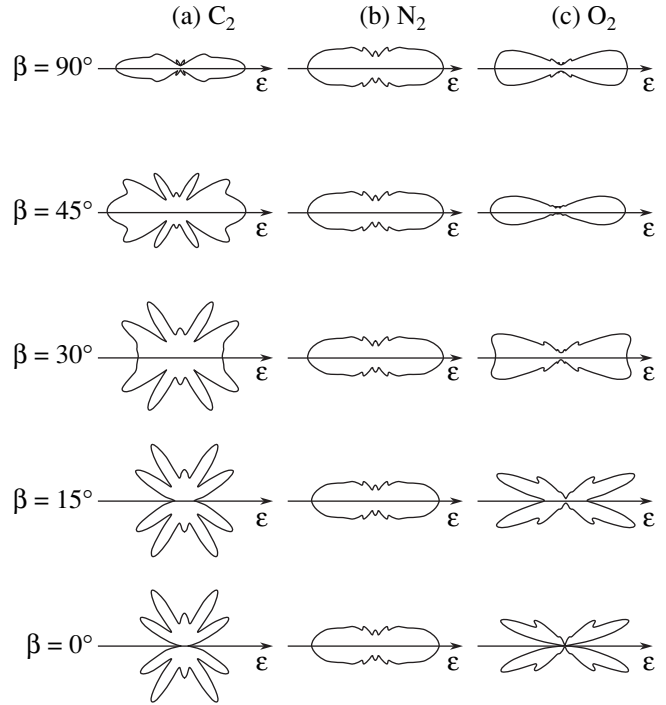


Fig. 3. Angular distributions for the diatomic molecules: (a) C_2 ($I_0 = 5 \times 10^{13} \text{ W/cm}^2$), (b) N_2 ($I_0 = 10^{14} \text{ W/cm}^2$), and (c) O_2 ($I_0 = 10^{14} \text{ W/cm}^2$). Each row corresponds to a different cone angle β , whose value is denoted on the left of the figure. Further laser parameters: $\lambda = 800 \text{ nm}$ and $\tau = 10 \text{ fs}$.

signatures identified in [9] are to different degrees of molecular alignment.

Figure 3 shows photoelectron angular distributions for diatomic molecules C_2 (left hand panels), N_2 (panels in the middle), and O_2 (right hand panels) for different degrees of alignment. In the figures, polar angles are measured from the laser polarization direction in the laboratory frame. In the case of complete alignment ($\beta = 0^\circ$), for C_2 and O_2 one observes a node along the polarization direction. The origin of this node lies in the symmetry of the ground-state wavefunctions of these

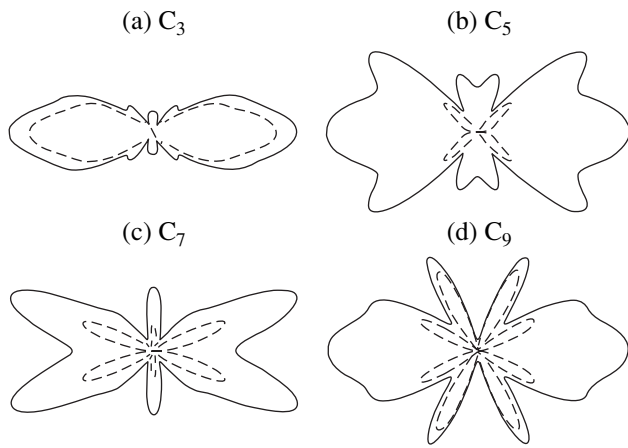


Fig. 4. Angular distributions for linear carbon clusters: (a) C_3 , $I_0 = 5 \times 10^{13} \text{ W/cm}^2$, (b) C_5 , $I_0 = 2 \times 10^{13} \text{ W/cm}^2$, (c) C_7 , $I_0 = 2 \times 10^{13} \text{ W/cm}^2$, and (d) C_9 , $I_0 = 10^{13} \text{ W/cm}^2$. A comparison is shown between the results obtained when contributions from all valence shells are taken into account (solid lines) and those arising from the HOMO only (dashed lines). Further laser parameters: $\lambda = 800 \text{ nm}$ and $\tau = 10 \text{ fs}$.

molecules. For both molecules, the HOMO is of π symmetry and possesses a nodal plane through the (body-fixed) molecular axis, leading to a vanishing photoelectron angular distribution along this axis. In a randomly oriented ensemble of such linear molecules (Fig. 3, $\beta = 90^\circ$), the minimum is washed out due to the summation of the contributions from the overwhelmingly larger number of molecules that are not oriented along the space-fixed axis. As can be expected, the minimum begins to appear below a certain cone angle even when the alignment is not exact. For the two molecules C_2 and O_2 , this angle is found to be about 30° .

In contrast, for a HOMO of σ symmetry, as in case of the N_2 molecule, there is no nodal plane along the molecular axis and therefore emission of the electrons along the polarization direction is not suppressed. Furthermore, the angular distributions do not change significantly for all the various cases of alignment considered here.

The node in the angular distributions has its origin in the π symmetry of the HOMO of the molecules. In order to investigate whether or not this signature also holds in the case of more complicated polyatomic molecules, we have performed calculations for linear carbon clusters.

In Fig. 4, angular distributions for carbon clusters are presented; results for ionization from the HOMO only (dashed line) are compared with those when contributions from the HOMO and the inner valence orbitals are taken into account (solid line). Clearly, for those carbon clusters whose HOMO are of π symmetry, namely, for C_5 , C_7 , and C_9 , the angular distributions exhibit the same signature as for the diatomic molecules as long as only the electron emission from the HOMO is considered. However, significant contributions from the inner valence shells destroy the symmetry signature for C_5 and C_9 , whereas some trace of the minimum survives for C_7 , when all the valence orbitals are considered in the calculations.

The results, presented in Fig. 5, show how sensitive the angular distributions for the carbon clusters are to different degrees of alignment. If there is a dominant contribution from (inner valence) orbitals of σ symmetry, the angular distributions are found to be rather independent of the degree of alignment (as in the case of N_2). On the other hand, for C_7 we see the typical change in the angular distributions from the “order” (aligned or predominantly aligned molecules in an ensemble) to

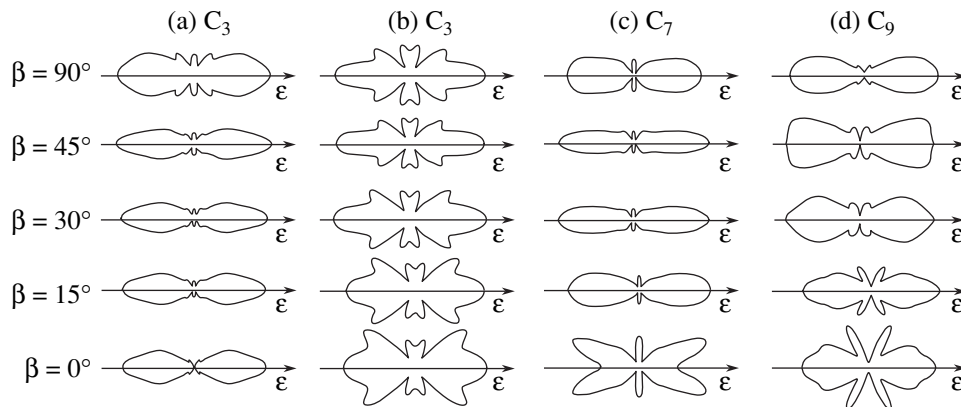


Fig. 5. Angular distributions for the carbon clusters: (a) C_3 , $I_0 = 5 \times 10^{13} \text{ W/cm}^2$, (b) C_5 , $I_0 = 2 \times 10^{13} \text{ W/cm}^2$, (c) C_7 , $I_0 = 2 \times 10^{13} \text{ W/cm}^2$, and (d) C_9 , $I_0 = 10^{13} \text{ W/cm}^2$. Comparison for different values of the cone angle β . Further laser parameters: $\lambda = 800 \text{ nm}$ and $\tau = 10 \text{ fs}$.

“disorder” case, as already discussed for the diatomic molecules C_2 and O_2 .

4. RESULTS FOR PHOTOELECTRON ENERGY DISTRIBUTIONS

Now we turn to the photoelectron energy spectra and investigate the signatures of molecular orbital symmetry and molecular orientations for the ionization of a homonuclear diatomic molecule. Figure 6 shows the energy spectra for N_2 for emission of the photoelectron along the direction of polarization. The laser parameters are $\lambda = 2400$ nm, $I_0 = 10^{14}$ W/cm², and $\tau = 10$ fs. Spectra (a) to (e) correspond to different cone angles β (Fig. 1), i.e., to different degrees of alignment in the ensemble of molecules. It is evident from the results that there is a deep minimum in the ATI spectrum in the case of complete alignment (Fig. 6e), which gradually disappears with an increase in the cone angle β .

The origin of this minimum and its disappearance during the increase in orientational disorder in the ensemble can be readily explained when rewriting Eq. (4). First, let us assume that the wavefunction of the molecule is written in the linear combination of atomic orbitals representation:

$$\Phi_i(\mathbf{r}; \mathbf{R}_1, \mathbf{R}_2) = \sum_{j=1}^{j_{\max}} a_j \phi_j(\mathbf{r}, -\mathbf{R}/2) + b_j \phi_j(\mathbf{r}, \mathbf{R}/2). \quad (7)$$

For a homonuclear, diatomic molecule, there are only two possibilities for the relation between the coefficients a_j and b_j , namely, $a_j = \pm b_j$. They correspond to a bonding (+) or an antibonding (−) symmetry of the molecular orbital. Using this, one obtains formula (4) in the following form [3]:

$$W^{(N)}(I, \hat{n}) = 2\pi N_e C_{\text{coul}} \sum_{N=N_0}^{\infty} k_N (U_p - N\omega)^2 \times \int_0^{2\pi} d\phi_{k_n} \int_0^{\pi} d\theta_{k_n} J_N^2 \left(\alpha_0 \cdot \mathbf{k}_N, \frac{U_p}{2\omega} \right) F(\mathbf{k}_N) \times \begin{cases} \sin^2(\mathbf{k}_N \cdot \mathbf{R}/2) & \text{for antibonding symmetry} \\ \cos^2(\mathbf{k}_N \cdot \mathbf{R}/2) & \text{for bonding symmetry,} \end{cases} \quad (8)$$

where R is the internuclear distance and $F(\mathbf{k}_N)$ is the function of \mathbf{k}_N and a_j .

The interference effects due to the antibonding versus bonding symmetry occur in Eq. (4) via the trigonometric factors \sin^2 and \cos^2 . From this, one can immediately see that energy spectra of homonuclear diatomic

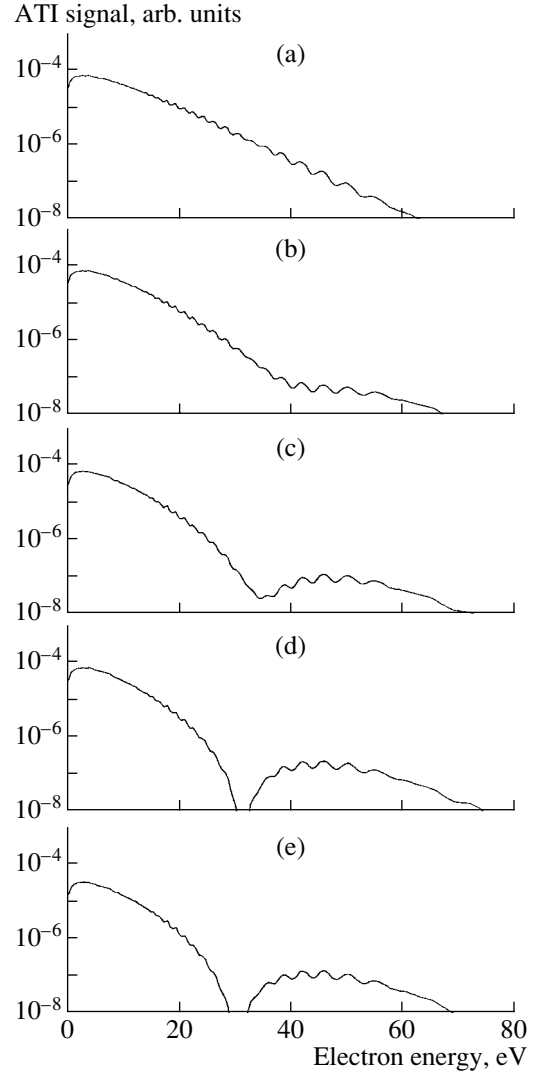


Fig. 6. Energy distributions for photoelectron emission along the polarization direction ($\hat{k}_N \parallel \epsilon$) from N_2 molecules for different degrees of alignment of the molecules in an ensemble: (a) $\beta = 90^\circ$, (b) $\beta = 45^\circ$, (c) $\beta = 30^\circ$, (d) $\beta = 15^\circ$, and (e) $\beta = 0^\circ$. Laser parameters: $\lambda = 2400$ nm, $I_0 = 10^{14}$ W/cm², and $\tau = 10$ fs.

molecules may be suppressed not only near the threshold [2] but also at certain higher energy values given by

$$= \frac{k_N^2}{2} \begin{cases} n^2 \pi^2 & \text{for antibonding symmetry} \\ n^2 \pi^2 / 4 & \text{for bonding symmetry,} \end{cases} \quad (9)$$

with $n = 1, 2, 3, \dots$. The above values depend on the internuclear distance, as well as on the directions of the electron emission \hat{k}_N , and of the orientation of the molecular axis \hat{n} through the angle between the molec-

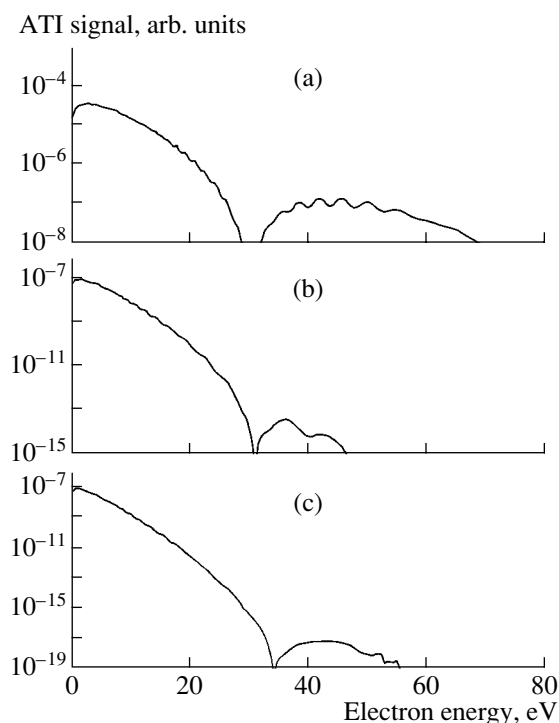


Fig. 7. Energy spectra for aligned N_2 molecules for different directions of photoelectron emission. The angle between the polarization direction and the electron emission direction is (a) 0° , (b) 10° , and (c) 20° , respectively; otherwise, same as in Fig. 6.

ular axis and the direction of the emission of the electron. Thus, the suppression should be most clearly visible for fixed directions of \hat{k}_N and \hat{n} .

The results in Fig. 6 are indeed in agreement with this observation. The deep minimum in Fig. 6e corresponds to the first minimum (Eq. (9), $n = 1$) predicted by the present theory for a molecule having a HOMO of bonding symmetry, such as N_2 . As the alignment within the molecular ensemble becomes incomplete, i.e., with an increase in β , the minimum becomes washed out and the energy spectrum for a randomly oriented ensemble of molecules becomes smooth and no longer shows any trace of the minimum. This is due to the average over the molecular orientations with respect to the fixed direction of photoelectron emission. The pronounced minimum in the ATI spectra at higher electron energies can be considered, on the one hand, as another trace of the interference effects between the subwaves from the two atomic centers, but it is, moreover, at the same time a signature of molecular alignment. Detection of this minimum can be further useful in view of molecular imaging, since its position in the energy spectrum determines the internuclear distance at the instant of ionization.

For the sake of comparison with future experiments, we finally present, in Fig. 7, the energy spectra for different directions of photoelectron emission in a com-

pletely aligned ensemble of N_2 molecules. As can be anticipated from Eq. (9), the position of the minimum depends on the angle between the internuclear axis and the unit vector of the photoelectron momentum.

We note further that the yields decrease quickly as soon as the photoelectron is observed at a nonzero angle with respect to the polarization direction. Therefore, the present interference effect and signature of alignment at higher electron energies should be best observed at rather long wavelengths and emission of the photoelectron along the polarization direction.

5. SUMMARY

In conclusion, we have presented results of our analysis on the signatures of molecular orbital symmetry and molecular alignment in the photoelectron angular and energy distributions resulting from strong-field ionization of diatomic molecules and linear carbon clusters. It is found that angular distributions depend strongly on the symmetry of the HOMO and on the degree of alignment of the molecular ensemble. A minimum along the polarization direction for molecules having a HOMO of π symmetry is identified as a signature of alignment.

Considering the photoelectron energy distributions, a second type of interference effects has been identified, namely, the minimum for higher energies appearing for homonuclear diatomic molecules. The position of this minimum in the ATI spectrum depends on the internuclear distance and the relative orientation of the direction of photoelectron emission and the molecular axis. Consequently, it provides another signature of alignment in an ensemble of molecules.

ACKNOWLEDGMENTS

A.J.-B. acknowledges the support of the Alexander von Humboldt-Stiftung (Bonn, Germany).

REFERENCES

1. E.g., M. Shapiro and P. Brumer, *Principles of the Quantum Control of Molecular Processes* (Wiley, Hoboken, N.J., 2003).
2. F. Grasbon, G. G. Paulus, S. L. Chin, *et al.*, *Phys. Rev. A* **63**, 041402(R) (2001).
3. J. Muth-Böhm, A. Becker, and F. H. M. Faisal, *Phys. Rev. Lett.* **85**, 2280 (2000).
4. J. Muth-Böhm, A. Becker, S. L. Chin, and F. H. M. Faisal, *Chem. Phys. Lett.* **337**, 313 (2001).
5. V. R. Bhardwaj, D. M. Rajner, D. M. Villeneuve, and P. B. Corkum, *Phys. Rev. Lett.* **87**, 253003 (2001).
6. M. Lein, N. Hay, R. Velotta, *et al.*, *Phys. Rev. Lett.* **88**, 183903 (2002); M. Lein, N. Hay, R. Velotta, *et al.*, *Phys. Rev. A* **66**, 023805 (2002); B. Shan, X. M. Tong, Z. Zhao, *et al.*, *Phys. Rev. A* **66**, 061401(R) (2002).
7. O. E. Alon, V. Averbukh, and N. Moiseyev, *Phys. Rev. Lett.* **80**, 3743 (1998); O. E. Alon, V. Averbukh, and

- N. Moiseyev, Phys. Rev. Lett. **85**, 5218 (2000); F. Ceccherini and D. Bauer, Phys. Rev. A **64**, 033 423 (2001).
8. M. Lein, P. Marangos, and P. L. Knight, Phys. Rev. A **66**, 051404(R) (2002).
 9. A. Jaroń-Becker, A. Becker, and F. H. M. Faisal, J. Phys. B **36**, L375 (2003).
 10. A. Jaroń-Becker, A. Becker, and F. H. M. Faisal, Phys. Rev. A (in press).
 11. J. J. Larsen, H. Sakai, C. P. Safvan, *et al.*, J. Chem. Phys. **111**, 7774 (1999).
 12. S. Banerjee, D. Mathur, and G. Ravindra Kumar, Phys. Rev. A **63**, 045401 (2001).
 13. D. H. Parker and R. B. Bernstein, Annu. Rev. Phys. Chem. **40**, 561 (1989).
 14. B. Friedrich and D. Herschbach, Nature **353**, 412 (1991); H. J. Loesch and A. Remscheid, J. Phys. Chem. **95**, 8194 (1991).
 15. B. Friedrich and D. Herschbach, Phys. Rev. Lett. **74**, 4623 (1995); W. Kim and P. M. Felker, J. Chem. Phys. **104**, 1147 (1996); C. M. Dion, A. Keller, O. Atabek, and A. D. Bandrauk, Phys. Rev. A **59**, 1382 (1999).
 16. J. J. Larsen, K. Hald, N. Bjerre, *et al.*, Phys. Rev. Lett. **85**, 2470 (2000).
 17. D. Normand, L. A. Lompré, and C. Cornaggia, J. Phys. B **25**, L497 (1992); M. Schmidt, S. Dobosz, P. Meynadier, *et al.*, Phys. Rev. A **60**, 4706 (1999); F. Rosca-Pruna and M. J. J. Vrakking, Phys. Rev. Lett. **87**, 153902 (2001); L. Quaglia, M. Brewczyk, and C. Cornaggia, Phys. Rev. A **65**, 031404(R) (2002).
 18. J. H. Posthumus, J. Plumridge, M. K. Thomas, *et al.*, J. Phys. B **31**, L553 (1998).
 19. Ch. Ellert and P. B. Corkum, Phys. Rev. A **59**, R3170 (1999).
 20. A. T. Georges and P. Lambropoulos, Phys. Rev. A **18**, 1072 (1978); M. P. Strand, J. Hansen, R.-L. Chien, and R. S. Berry, Chem. Phys. Lett. **59**, 205 (1978); S. C. Althorpe and T. Seideman, J. Chem. Phys. **110**, 147 (1999); J. A. Davies, R. E. Continetti, D. W. Chandler, and C. C. Hayden, Phys. Rev. Lett. **84**, 5983 (2000); J. G. Underwood and K. L. Reid, J. Chem. Phys. **113**, 1067 (2000); M. Tsubouchi, B. J. Whitaker, Li Wang, *et al.*, Phys. Rev. Lett. **86**, 4500 (2001).
 21. L. V. Keldysh, Zh. Eksp. Teor. Fiz. **47**, 1945 (1964) [Sov. Phys. JETP **20**, 1307 (1965)]; F. H. M. Faisal, J. Phys. B **6**, L89 (1973); H. R. Reiss, Phys. Rev. A **22**, 1786 (1980).
 22. F. H. M. Faisal, *Theory of Multiphoton Processes* (Plenum, New York, 1987).
 23. M. W. Schmidt *et al.*, J. Comput. Chem. **14**, 1347 (1993).
 24. K. P. Huber, and G. Herzberg, *Constants of Diatomic Molecules* (data prepared by J. W. Gallagher and R. D. Johnson, III) in NIST Chemistry WebBook, NIST Standard Reference Database Number 69, Eds. by P. J. Lindstrom and W. G. Mallard (Natl. Inst. of Standards and Technology, Gaithersburg, MD, 2003), 20899; webbook.nist.gov. (2003).
 25. A. van Orden and R. J. Saykally, Chem. Rev. **98**, 2313 (1998).
 26. Ch. Lifshitz, Int. J. Mass Spectrom. **200**, 423 (2000).
 27. M. S. Deleuze, M. G. Giuffreda, J.-P. François, and L. S. Cederbaum, J. Chem. Phys. **111**, 5851 (1999).